IEEE Access
Multidisciplinary ⋮ Rapid Review ⋮ Open Access Journal

Received 1 December 2023, accepted 10 December 2023, date of publication 13 December 2023,
date of current version 19 December 2023.

Digital Object Identifier 10.1109/ACCESS.2023.3342291

RESEARCH ARTICLE

Integration Design of Compact Balun Filters and Duplexing Balun Filter With Arbitrary Frequency-Selective Response

CHI-FENG CHEN, (Member, IEEE), YI-FANG TSAI, BAI-HONG CHEN, RUO-YIN YANG, AND YU-SHENG ZENG

Department of Electrical Engineering, Tunghai University, Taichung 40704, Taiwan

Corresponding author: Chi-Feng Chen (cfchen@thu.edu.tw)

This work was supported in part by the Ministry of Science and Technology, Taiwan, under Grant MOST 106-2221-E-029-001; and in part by the National Science and Technology Council, Taiwan, under Grant NSTC 112-2221-E-029-009.

ABSTRACT In this paper, a multifunctional microwave balun filter and balun diplexer design method is introduced. Through the proposed novel coupling structure and the use of miniaturized grid resonators, not only can the overall circuit area be reduced, but also features such as frequency selection, out-of-phase power splitting, and frequency division can be realized. This study actually designed and fabricated two balun filters and one balun diplexer. The simulated predictions of their frequency responses are in good agreement with the measurement results, validating the feasibility of the proposed technique. The results show that the circuit area of the developed balun filter and balun diplexer is approximately $0.08\lambda_g^2$ and $0.136\lambda_g^2$, respectively. They also exhibit satisfactory performance, with in-band insertion loss < 0.7dB, in-band return loss > 15dB, port-to-port isolation > 30dB, maximum in-band magnitude imbalance of 0.9dB, and in-band phase imbalance of $180° \pm 8°$.

INDEX TERMS Bandpass filters, baluns, diplexers, microstrip, multifunctional components.

I. INTRODUCTION

In recent years, a concerted effort has been made by numerous research teams to reduce the spatial footprint of circuits within communication systems and curtail production costs. One approach involves the integration of multiple microwave circuit functions into a single component. For instance, in [1], [2], [3], [4], [5], [6], and [7], there's a fusion of the bandpass filter and power divider, resulting in what's termed a filtering power divider. In [1], a quasi-elliptic function filter replaces the traditional quarter-wavelength transformer in the Wilkinson power divider, coupled with a zero-degree feeding structure to achieve improved frequency selectivity. Reference [2] adopts a stepped impedance interdigital coupling element to supplant the quarter-wavelength transformer in the conventional Wilkinson power divider, thereby achieving a bandpass response. References [3], [4], and [5] present dual-band and high-isolation filtering power dividers, based on coupled resonator technology. In [6] and [7], a frequency-tunable mechanism is introduced to the filtering power dividers. Reference [8] employs discriminating coupling to achieve a filtering power divider with a wide stopband response.

Baluns are three-port networks that convert balanced signals to unbalanced signals. In [9], [10], [11], [12], [13], [14], [15], [16], [17], [18], [19], [20], [21], and [22], various approaches for integrating bandpass filter with balun into a single component, known as a balun filter or filtering balun, are discussed. References [9], [10], [11], [12], [13], and [14] employ specific boundary conditions to transform a four-port balanced-to-balanced bandpass filter into a three-port balun filter with the aim of achieving both high common-mode suppression and circuit miniaturization. References [15], [16], and [17] utilize the voltage distribution characteristics of

The associate editor coordinating the review of this manuscript and approving it for publication was Dusan Grujić.

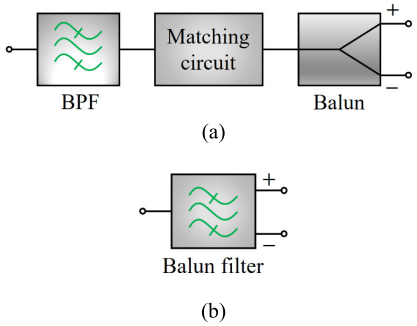

FIGURE 1. Block diagrams. (a) Cascade of a bandpass filter, a matching circuit, and a balun; (b) balun filter.

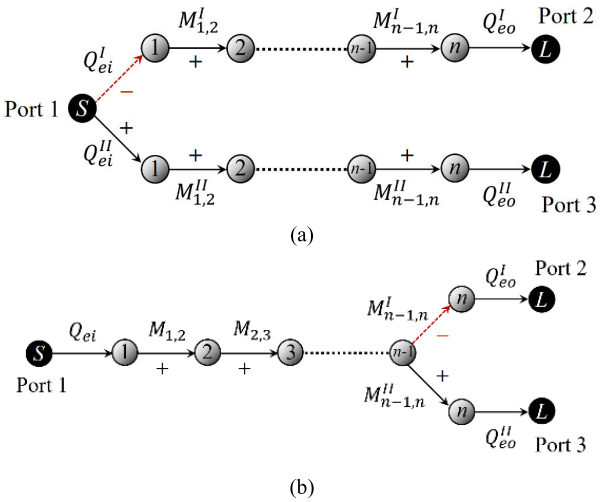

FIGURE 2. Balun filters with *n*th-order Chebyshev bandpass response. (a) Type I and (b) Type II.

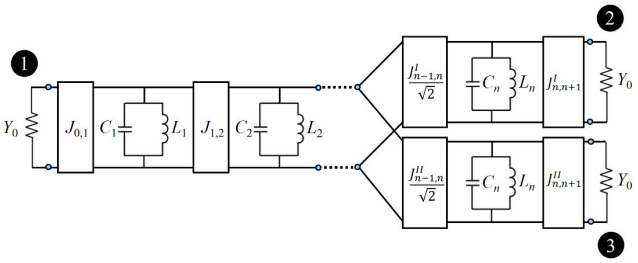

FIGURE 3. Equivalent circuit of the balun filter (Type II).

open-circuited half-wavelength microstrip lines to generate out-of-phase signals for balun filter design. Reference [18] employs dual-mode resonators to realize balun filters, which are then combined with quasi-Yagi antennas. In [20], a method for direct synthesis is introduced to design and investigate wideband filtering baluns, utilizing a compact structure of triple-mode stacked composite resonators. In [21], an reconfigurable wideband filtering balun is introduced, offering tunable dual-notched bands. This is achieved through the utilization of coplanar waveguide (CPW)-to-slot transitions and varactor-loaded shorted-slots. In [22], a balun with filtering capabilities is introduced, and it is built upon a spoof surface plasmon polariton (SSPP) structure. This SSPP structure consists of a symmetric H-shaped periodic metallic strip, two different microstrip-slotline cross-coupling structures, and the transitional structure connecting them.

Additionally, balanced-to-unbalanced diplexers, known as balun diplexers or duplexing balun filters, are discussed in [23], [24], [25], [26], and [27]. In [23], balun diplexers were designed by leveraging the voltage distribution properties of microstrip lines at the input and output ends, along with appropriate placement of resonators. In [24], a balun diplexer is created, incorporating a hybrid combination of microstrip and slot-line resonator structures. This design achieves wideband common-mode (CM) suppression. In [25], a set of designs for balanced and unbalanced cavity diplexers is presented. To reduce the overall size, a strategy is implemented wherein a triple-mode resonator is shared, and the matching network is omitted. In [26], the research focuses on designing a compact unbalanced-/balanced-to-unbalanced diplexer. The utilization of a dual-mode dielectric resonator effectively reduces the circuit size. In [27], an innovative integrated design of a filtering balun diplexer with enhanced output isolation performance was explored. The substantial improvement in output isolation was achieved through the cancellation of electric and magnetic couplings. To achieve circuit miniaturization, a filtering balun-diplexer based on dual-mode coupled-line-loaded hairpin ring resonators was proposed in [28].

Integrating the functionalities of multiple microwave circuits into a single component or developing microwave circuits with multifunctional characteristics has been one of the hottest research topics in recent years. However, the circuits published in the current literature still have some shortcomings that need improvement, such as excessive circuit size, as well as deficiencies in isolation, stopband response, and frequency selectivity. These limitations restrict their future development and application. Therefore, in this study, we have developed smaller-sized balun filters. On the other hand, we have also introduced an innovative miniaturized balun diplexer, which integrates the characteristics of bandpass filter, balun, and diplexer, into a single component. This can significantly reduce the number of circuits in wireless communication systems and consequently reduce the overall circuit footprint. Moreover, the proposed topology can offer arbitrary frequency-selective responses.

The rest of this paper is organized as follows. Section II presents the design and implementation for the proposed balun filters in detail. In Section III, a design approach for the balun diplexer is presented, and its feasibility is verified through practical implementation. Furthermore, its performance is compared with state-of-the-art balun diplexers. Finally, Section IV presents the conclusion.

II. DESIGN AND IMPLEMENTATION OF BALUN FILTERS

As shown in Fig. 1(a) and (b), integrating the bandpass filter and the balun into a single component can effectively

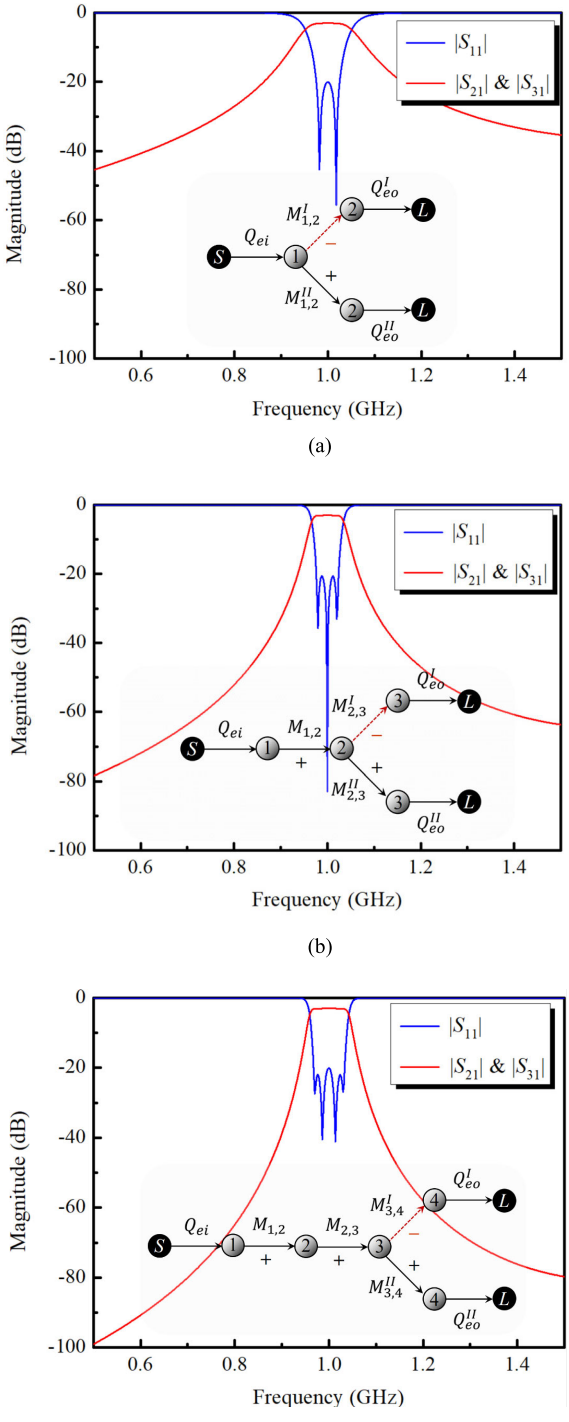

FIGURE 4. Theoretical frequency responses for the proposed balun filters with (a) second-order, (b) third-order, and (c) fourth-order Chebyshev responses (0.04321-dB passband ripple).

reduce the circuit footprint of microwave wireless communication systems. There are two feasible coupling structures for the balun filter, as illustrated in Fig. 2(a) and (b). The nodes labeled 1 to n represent resonator circuits, while nodes S and L respectively denote the source and load ports.

TABLE 1. Specifications of the balun filters.

	Balun filter I	Balun filter II
Center frequency (GHz)	0.825	1.18
Fractional bandwidth (%)	7.5	8
Filter order	3	3
Frequency response	Chebyshev (0.04321-dB ripple)	

TABLE 2. Theoretical coupling coefficients and external quality factors.

	Balun filter I	Balun filter II
M_{12}	0.077	0.083
M^{I}_{23}	–0.055	–0.058
M^{II}_{23}	0.055	0.058
Q_{ei} $(= Q^{I}_{eo} = Q^{II}_{eo})$	11.35	10.65

The connecting lines between nodes represent the coupling paths. In the Type I circuit [as shown in Fig. 2(a)], the primary approach involves using distributed coupling techniques at the input port (Port 1) to couple the signal into two nth-order Chebyshev bandpass filters with identical frequency responses. The signals are then separately output from Ports 2 and 3. Proper design of the coupling at the input structure is crucial, ensuring that these two coupling paths have a 180-degree phase difference (represented in the diagram by solid and dashed lines or by the positive and negative signs of coupling coefficients) so that the signals at the two output ports have a 180-degree phase difference. In fact, the design concept in [15], [16], and [17] is based on utilizing this type of technique to achieve a balun filter. However, this type of circuit requires a total of $2n$ resonators, which inevitably results in a larger circuit footprint. In the Type II circuit [as shown in Fig. 2(b)], the coupling path splits into two branches after the second-to-last resonator, and the coupling coefficients must satisfy $M^{I}_{n-1,n} = -M^{II}_{n-1,n}$. As seen in the diagram, this structure allows two bandpass filters to share $n-1$ resonators, thus requiring only $n+1$ resonators to compose this configuration. In other words, the structure in Fig. 2(b) significantly reduces the circuit footprint, and its equivalent circuit is depicted in Fig. 3. In practical design, the simplest method to achieve a 180-degree phase difference between the two couplings is by utilizing electric coupling and magnetic coupling between resonators, as outlined in [29].

To circuit miniaturization, the upcoming research will select the Type II structure for the design of the balun filter. To achieve equal power output and an nth-order Chebyshev passband response, the required coupling coefficients and the external quality factors at the input and output ports can be calculated using the following formulas:

$$M_{m,m+1} = \frac{FBW}{\sqrt{g_m g_{m+1}}}, \quad 1 \le m \le n-2 \tag{1}$$

$$M^{I}_{n-1,n} = -M^{II}_{n-1,n} = \frac{FBW}{\sqrt{2 g_{n-1} g_n}} \tag{2}$$

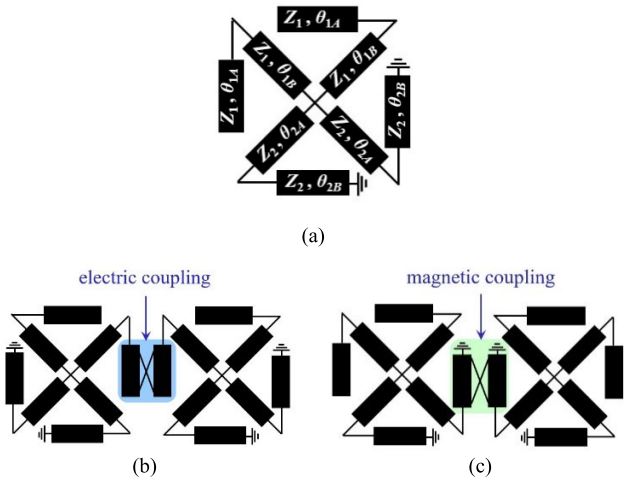

FIGURE 5. (a) Circuit model of a grid resonator. (b) Electric coupling. (c) Magnetic coupling.

$$Q_{ei} = Q_{eo} = \frac{g_0 g_1}{FBW} \tag{3}$$

where FBW represents the fractional bandwidth; g-value represents the element value for Chebyshev lowpass prototype filters, and when the filter order and passband ripple are specified, its value can be obtained by [29].

For example, when given a center frequency of 1 GHz, a fractional bandwidth of 5%, and a passband ripple of 0.04321 dB (equivalent to a return loss of 20 dB), the frequency response of the ideal circuit is shown in Fig. 4. It can be observed that the proposed concept can indeed integrate both the bandpass filter and balun into a single component, while also offering advantages in terms of miniaturization in its structure. Furthermore, this technology can achieve frequency-selective responses of arbitrary orders.

In order to further reduce the circuit size in real implementation, a folded open- and short-ended stub-loaded resonator, alternatively named grid resonator, was employed in this design. The circuit model of the grid resonator is illustrated in Fig. 5(a). As seen, the resonator is compact (approximately one-eighth of a wavelength by one-eighth of a wavelength) and is composed of two open-circuited stubs with characteristic impedance of Z_1 and electrical length of $(\theta_{1A}+\theta_{1B})$ as well as two short-circuited stubs with characteristic impedance of Z_2 and electrical length of $(\theta_{2A} + \theta_{2B})$. For simplified consideration, it is preferable to choose $Z_1 = Z_2$. The resonance condition can be expressed by the equation:

$$\cot(\theta_{1A} + \theta_{1B}) = \tan(\theta_{2A} + \theta_{2B}) \tag{4}$$

Actually, the grid resonator could be regarded as a quarter-wavelength resonator at the fundamental mode. This kind of resonator could bring not only compact size but also significant flexibility in designing the coupled-resonator-based circuits. For example, the electric coupling can be acquired if the open-ended transmission lines of two grid resonators are closely placed, as shown in Fig. 5(b), whereas the magnetic coupling can be acquired if the short-ended transmission lines of two grid resonators are closely placed, as shown in Fig. 5(c).

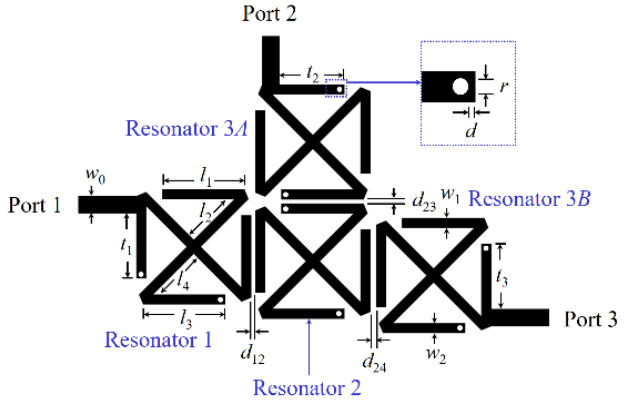

FIGURE 6. Layout of the microstrip balun filter (not to scale).

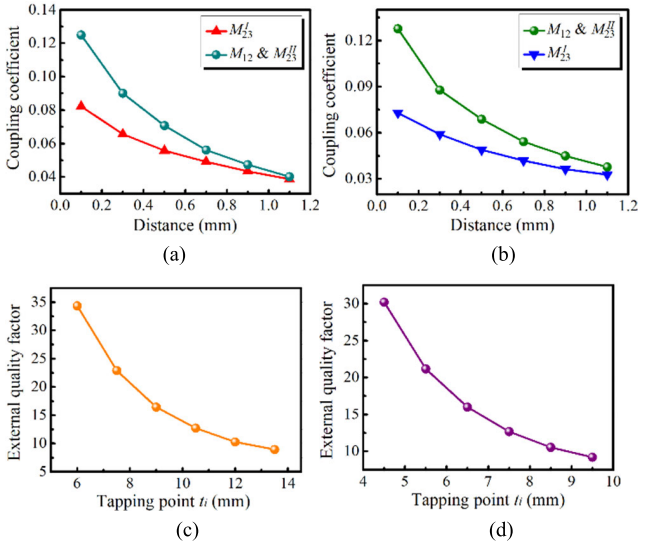

FIGURE 7. Design curves. (a) Extracted coupling coefficients for balun filter I. (b) Extracted coupling coefficients for balun filter II. (c) Extracted external quality factors for balun filter I. (d) Extracted external quality factors for balun filter II.

To verify the proposed concept, two balun filters were designed according to the given specifications as listed in Table 1. The required coupling coefficients and external quality factors for the two balun BPFs, calculated from (1)-(3), are summarized in Table 2. Rogers RO4003 substrate, which exhibited a loss tangent δ of 0.0027, thickness of 60 mil, and relative dielectric constant ϵ_r of 3.55, is used. To determine the structural parameters of the balun filter, its design method can utilize traditional coupled-resonator circuit technology [29]. The first step is to determine the physical dimensions of each grid resonator based on (4). The resonant frequency of each resonator must correspond to the center frequency of the filter. Once the structural parameters of all grid resonators are determined, the next step is to determine the distances between adjacent

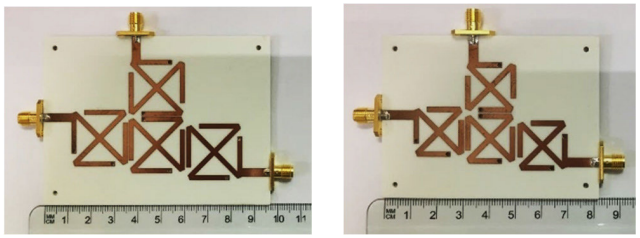

(a) (b)

FIGURE 8. Photographs of the designed balun filters. (a) balun filter I (0.825 GHz) and (b) balun filter II (1.18 GHz).

TABLE 3. Physical parameters of the balun filter I.

l_1	l_2	l_3	l_4	w_0	w_1
17	12	17	12	3.53	2
w_2	d_{12}	d_{23}	d_{24}	t_1	t_2
2	0.4	0.4	0.74	13.47	13.47
t_3	r	d			
13.47	1.6	0.2			

TABLE 4. Physical parameters of the balun filter II.

l_1	l_2	l_3	l_4	w_0	w_1
12.5	8.5	12.5	8.5	3.53	2
w_2	d_{12}	d_{23}	d_{24}	t_1	t_2
2	0.5	0.45	0.92	8.97	8.97
t_3	r	d			
8.97	1.6	0.2			

resonators and the position of the tapping point of the input/output (I/O) feeding line based on the required coupling coefficients and external quality factors, respectively. For synchronously tuned coupled resonators, even-odd mode analysis can be employed to examine this symmetric circuit. By introducing electrical walls or magnetic walls in the symmetrical plane, their respective resonant frequencies can be determined. Subsequently, based on the definition of coupling coefficients, the relationship between coupling coefficients and resonant frequencies can be derived as follows:

$$M = \pm \frac{f_{p2}^2 - f_{p1}^2}{f_{p2}^2 + f_{p1}^2} \tag{5}$$

The terms f_{p1} and f_{p2} represent the lower and upper fundamental resonant frequencies of the two coupled resonators when experiencing weak coupling. The sign of the coupling coefficient is related to the actual coupling structure and its phase variations. On the other hand, in the case of a singly loaded resonator, calculating the phase variation of return loss allows for the determination of the external quality factor using the following equation:

$$Q_e = \frac{\omega_0}{\Delta\omega_{\pm 90^\circ}} \tag{6}$$

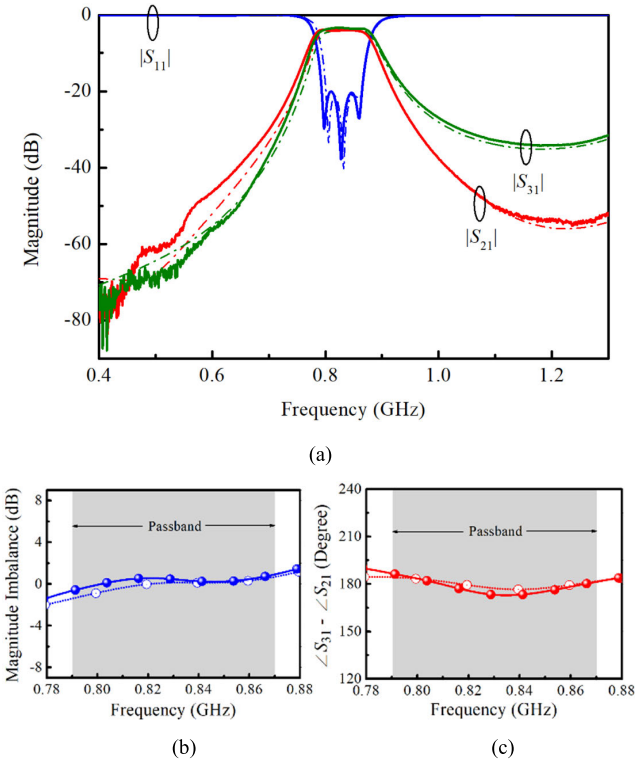

FIGURE 9. Simulated (Dashed lines) and measured (solid lines) performance of the balun filter I. (a) $|S_{11}|$, $|S_{21}|$, and $|S_{31}|$; (b) magnitude imbalance; (c) phase difference.

where ω_0 represents the resonant frequency of the resonator, and $\Delta\omega_{\pm 90^\circ}$ is the 180-degree bandwidth centered around the resonant frequency.

The proposed balun filter's design steps are as follows:

Step 1) Define specifications, including center frequency, bandwidth, filter order, passband ripple, etc., and calculate the required coupling coefficients and external quality factors using equations (1) to (3).

Step 2) Determine the structural parameters of the grid resonator based on the given center frequency.

Step 3) Decide the distances between adjacent resonators and the I/O coupling structure based on the required coupling coefficients and external quality factors.

Step 4) If necessary, perform structural parameter adjustments to ensure that the frequency response meets the specified specifications.

Fig. 6 shows the microstrip structure of the proposed balun filter, which consists of four grid resonator. In fact, this balun filter can be considered as composed of two third-order Chebyshev bandpass filters, with resonators 1 and 2 being shared by both filters. In this configuration, the coupling between resonators 1 and 2 and between resonators 2 and 3B is achieved through electrical coupling (indicated by positive coupling coefficients), while the coupling between resonators 2 and 3A is achieved through magnetic coupling (indicated by negative coupling coefficients). This arrangement results in the signals at the two output ports exhibit

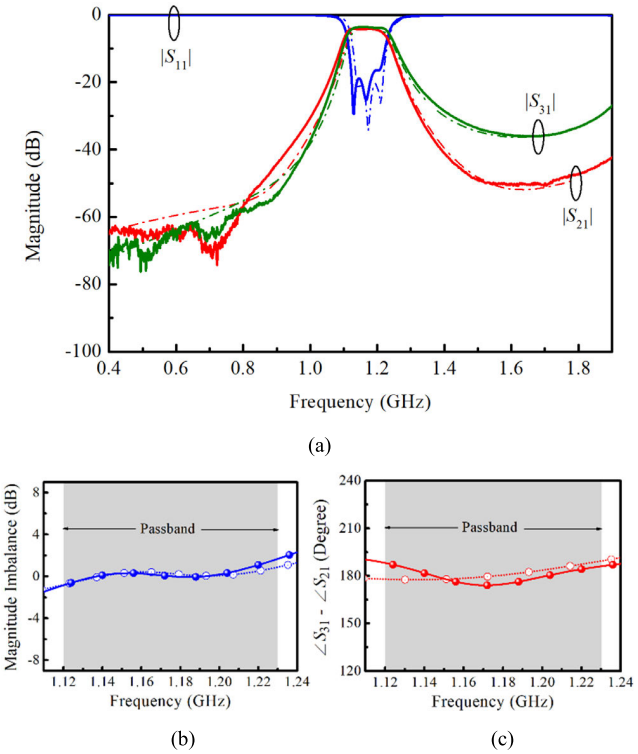

FIGURE 10. Simulated (Dashed lines) and measured (solid lines) performance of the balun filter II. (a) $|S_{11}|$, $|S_{21}|$, and $|S_{31}|$; (b) magnitude imbalance; (c) phase difference.

TABLE 5. Comparison of state-of-the-art balun filters.

	CF (GHz)	FBW (%)	IL (dB)	RL (dB)	FO	Size (λ_g^2)
This work (I)	0.825	7.5	0.7	> 20	3	0.06
This work (II)	1.18	8	0.6	> 16	3	0.08
[15]	1	30	0.8	> 20	3	0.186
[16]	2	11	0.8	> 20	2	0.125
[17]	2.4	5.8	0.7	> 18	2	0.172
[20]	2.95	109	0.9	> 14	3	N/A
[21]	2.16	102.6	0.4	> 15	3	0.258
[22]	2	12.5	1.1	> 10	N/A	N/A

CF: central frequency, FBW: fractional bandwidth, IL: insertion loss, RL: return loss, FO: filter order

an out-of-phase effect. Fig. 7(a) and (b) show the extracted coupling coefficients with different distance between two adjacent resonators and Fig. 7(c) and (d) show the extracted external quality factors with different position of the tapping point of the feeding line. Subsequently, the distances between adjacent resonators and the positions of the tapping point of the feeding line can be determined according to the required coupling coefficients and external quality factors, respectively.

The photographs of the designed balun filters I and II are shown in Fig. 8(a) and (b), respectively, with all their physical parameters listed in Tables 3 and 4. The circuit

TABLE 6. Specifications of the duplexing balun filter.

	Channel 1	Channel 2
Center frequency (GHz)	0.825	1.18
Fractional bandwidth (%)	7.5	8
Filter order	3	3
Insertion loss (dB)	< 1	
Isolation (dB)	> 30	
Frequency response	Chebyshev (0.04321-dB ripple)	

area of balun filter I measures 72.5mm × 47.9mm, which is equivalent to only $0.3\lambda_g \times 0.2\lambda_g$, where λ_g represents the guided wavelength at the center frequency. Balun filter II has a circuit area of 57.6mm × 38.1mm, which is equivalent to only $0.35\lambda_g \times 0.23\lambda_g$.

The simulation and measurement results for balun filter I are shown in Fig. 9(a), (b), and (c), with measurements performed using the Agilent N5230A vector network analyzer. The measurement results indicate that the return loss ($-20\log|S_{11}|$) within the passband is above 20 dB. The insertion losses ($-20\log|S_{21}|$ and $-20\log|S_{31}|$) within the passband are approximately 3 + 0.7 dB, with the losses primarily attributed to conductor losses. Furthermore, the measurement of $|S_{31}| - |S_{21}|$ within the passband is 0 ± 0.9 dB, and the measurement of $\angle S_{31} - \angle S_{21}$ within the passband is $180° \pm 8°$. On the other hand, the simulation and measurement results for balun filter II are depicted in Fig. 10(a), (b), and (c). According to the measurement results, the return loss within the passband is greater than 16 dB. The insertion losses within the passband are approximately 3 + 0.58 dB, with the primary contribution being conductor losses. Additionally, the measurement of $|S_{31}| - |S_{21}|$ within the passband is 0 ± 0.9 dB, and the measurement of $\angle S_{31} - \angle S_{21}$ within the passband is $180° \pm 7°$.

Furthermore, as the developed balun filter is constructed using grid resonators, its spurious passband occurs at three times the center frequency. In other words, this balun filter benefits from a wide stopband. Overall, the simulated predictions align closely with the measured results, indicating the feasibility of the proposed design concept. Table 5 provides a comparison between the developed balun filters and balun filters published in recent years. From the table, it is evident that the circuit area of the developed balun filter is the smallest.

III. DESIGN AND IMPLEMENTATION OF DUPLEXING BALUN FILTER

A typical frequency-division duplexing transceiver, as shown in Fig. 11(a), is primarily composed of two baluns, two bandpass filters, and three matching circuits. As evident from the diagram, such a combination inevitably leads to a larger circuit area. Therefore, if it is possible to integrate these circuits into one, namely a duplexing balun filter as illustrated

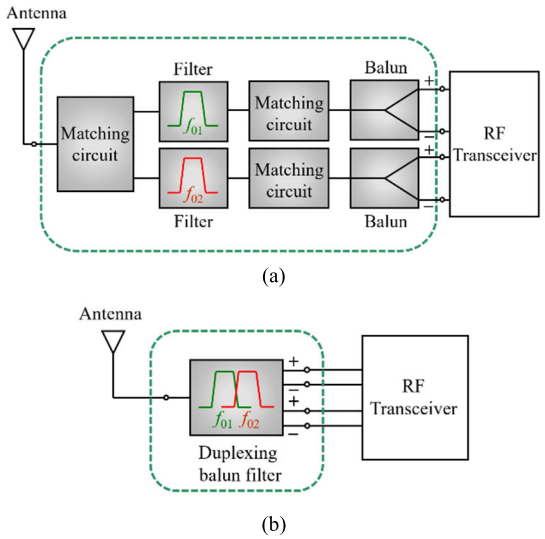

FIGURE 11. The schematic diagram of (a) the conventional and (b) the proposed frequency-division duplexing transceiver.

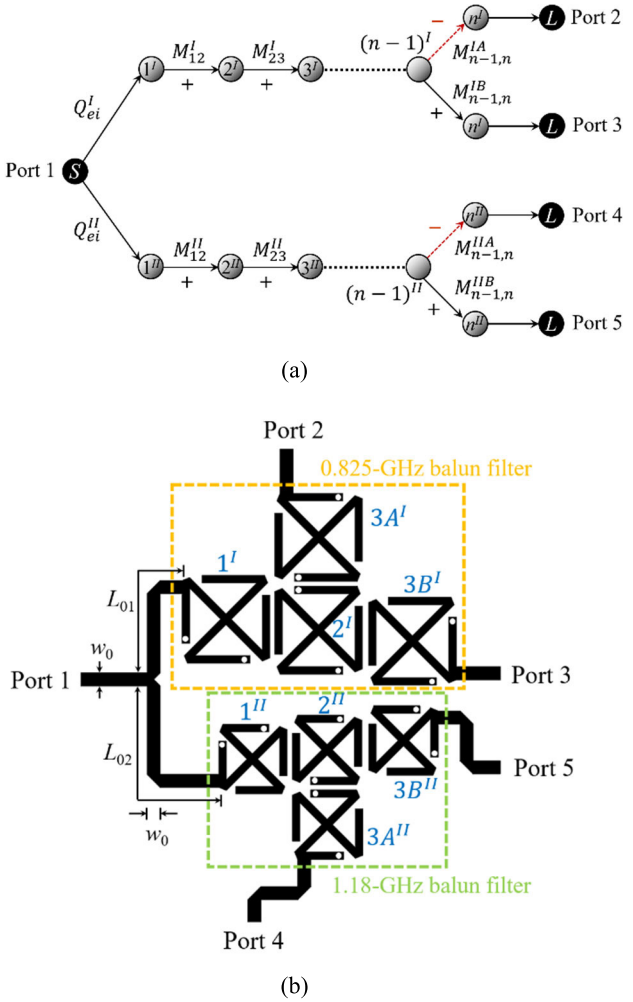

FIGURE 12. (a) Coupling structure of the duplexing balun filter with*n*th-order Chebyshev bandpass response. (b) Layout of the microstrip duplexing balun filter with third-order Chebyshev bandpass response.

in Fig. 11(b), it can effectively reduce the circuit area required for this transceiver.

Fig. 12(a) depicts the coupling structure of the proposed duplexing balun filter with nth-order Chebyshev bandpass response. In the diagram, each node represents a resonator circuit; S and L denote the source and load ports, respectively. The connecting lines between nodes represent the coupling paths. In fact, this circuit is composed of two balun filters operating at different frequencies. In the coupling structure diagram, the resonant frequencies labeled as I and II for channels 1 and 2 must be designed to correspond to the center frequencies of these channels. The theoretical values of coupling coefficients and external quality factors can be calculated from equations (1) to (3). Please note that the coupling coefficients between the last two resonators must satisfy $M^{IA}_{n-1,n} = -M^{IB}_{n-1,n}$ and $M^{IIA}_{n-1,n} = -M^{IIB}_{n-1,n}$ to achieve an out-of-phase effect in the output signals of these two channels. Furthermore, since this duplexing balun filter only requires $2n+2$ resonators to be constructed, and if these resonators can be implemented using the aforementioned grid resonators, it is expected that the overall circuit area can be significantly reduced.

The specifications of the designed duplexing balun filter are presented in Table 6. The substrate used is Rogers RO4003, with a dielectric constant of 3.55, thickness of 60 mil, and a loss tangent of 0.0027. Fig. 12(b) illustrates the microstrip structure of this duplexing balun filter with a third-order Chebyshev bandpass response. This structure is composed of a total of eight grid resonators, where resonators 1^I, 2^I, $3A^I$, and $3B^I$ resonate at the center frequency of channel 1 (i.e., 0.825 GHz), and resonators 1^{II}, 2^{II}, $3A^{II}$, and $3B^{II}$ resonate at the center frequency of channel 2 (i.e., 1.18 GHz). The coupling between resonators 2^I and $3A^I$, as well as between resonators 2^{II} and $3A^{II}$, is achieved through magnetic coupling, while the coupling between the other resonators is accomplished through electrical coupling. These two balun filters operating at different frequency bands can be individually designed, and then integrated using a T-junction matching circuit. The input impedance seen by each balun filter at the T-junction must meet two criteria. It should provide an impedance match at the center frequency of the respective balun filter while maintaining an open circuit at the center frequency of the other balun filter sharing the same junction. Hence, parameters L_{01} and L_{02} are adjusted to meet the conditions mentioned above. As this structure provides independent coupling paths at each operating frequency, it significantly enhances the design flexibility of circuit structural parameters and reduces the design complexity. Designers can also properly incorporate additional resonators to further develop multi-channel or higher-frequency selectivity balun multiplexers. In summary, the proposed duplexing balun filter is a component that integrates the characteristics of bandpass filters, baluns, and diplexers, allowing for a substantial reduction in the

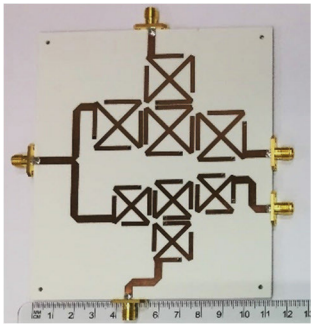

FIGURE 13. Photograph of the fabricated duplexing balun filter.

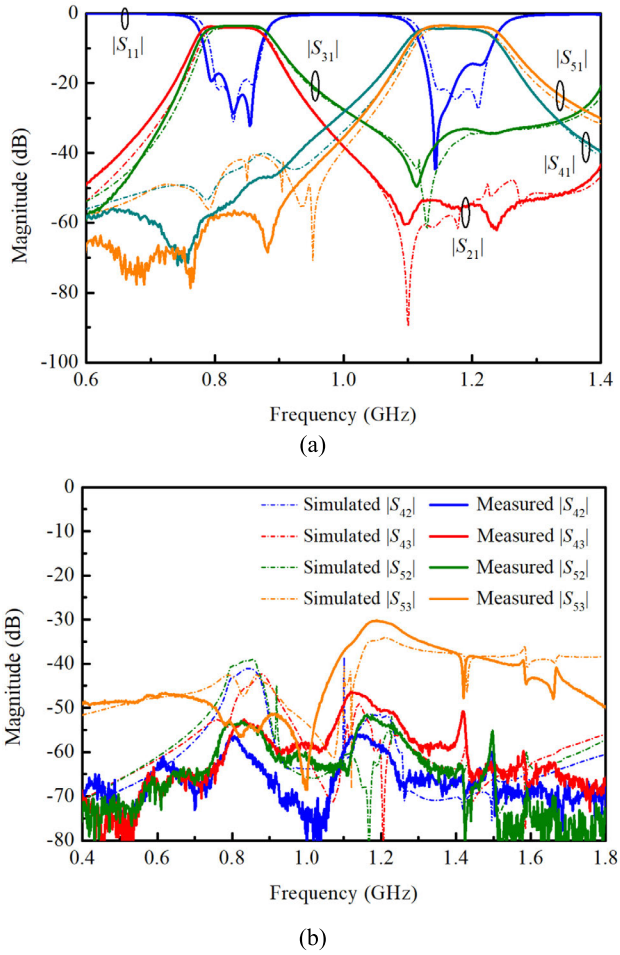

FIGURE 14. Simulated (Dashed lines) and measured (solid lines) performance of the duplexing balun filter. (a) Power transmission and reflection; (b) isolation performance.

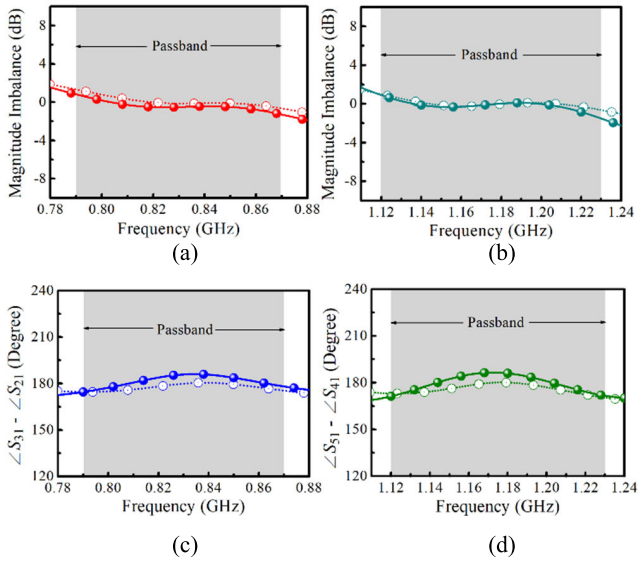

FIGURE 15. Measurement (solid lines) and simulation (Dashed lines) results of the proposed duplexing balun filter. (a) Magnitude imbalance for channel 1; (b) magnitude imbalance for channel 2; (c) phase difference for channel 1; (d) phase difference for channel 2.

TABLE 7. Comparison of state-of-the-art duplexing balun filters.

	CF (GHz)	FBW (%)	IL (dB)	Iso (dB)	Size (λ_g^2)	DF
This work	0.825, 1.18	7.5, 8	0.7, 0.6	> 30	0.136	high
[13]	1.84, 2.45	10, 10	1.42, 1.77	> 30	0.182	medium
[14]	1, 1.2	10.5, 10.4	2.2, 2.35	> 46	0.175	medium
[23]	2.59, 5.41	9.26, 5.73	2.7, 3.7	> 40	0.185	high
[24]	1.92, 2.45	11.5, 8.2	1.56, 2.28	> 25	0.308	medium
[27]	1, 1.6	5, 5	2.9, 3.8	> 20	0.263	medium
[28]	2.45, 5.05	4.1, 3.6	1.2, 1.6	> 39	0.034	low

CF: central frequency, FBW: fractional bandwidth, IL: insertion loss, Iso: isolation, DF: design freedom

circuit area it occupies within a frequency-division duplexing transceiver system. In addition, due to the flexible design of the proposed structure, balanced ports can be configured in close proximity or separated, making it adaptable to various applications.

The structural parameters of these two balun filters are shown in Tables 3 and 4, while the structural parameters of the T-junction matching circuit are as follows: $L_{01} = 27.5$mm, $L_{02} = 40$mm, and $w_0 = 3.53$mm. The circuit area of the duplexing balun filter is 82mm×97.2mm, which is equivalent to only $0.34\lambda_g \times 0.4\lambda_g$, where λ_g represents the guided wavelength at the center frequency of the first channel.

Fig. 13 shows a circuit photograph of this duplexing balun filter, and its simulated and measured results are presented in Fig. 14(a) and (b), and Fig. 15(a)–(d). The measurement results demonstrate that the return loss is greater than 15 dB in both passbands, and the insertion loss in the low and high-frequency channels is approximately 3 + 0.71 dB and 3 + 0.6 dB, respectively, mainly due to conductor losses. Additionally, the isolations of this circuit ($-20\log|S_{42}|$, $-20\log|S_{43}|$, $-20\log|S_{52}|$, and $-20\log|S_{53}|$) are greater than 30 dB within both operating frequency bands, and the stopband attenuation is greater than 40 dB. Furthermore, within the first channel, the measured $|S_{31}| - |S_{21}|$ is approximately 0 ± 0.9 dB, and the phase difference $\angle S_{31} - \angle S_{21}$ is approximately $180° \pm 6°$. In the second

channel, the measured $|S_{41}| - |S_{51}|$ is around 0 ± 0.9 dB, and the phase difference $\angle S_{51} - \angle S_{41}$ is approximately $180° \pm 7°$. The discrepancies between the amplitude and phase imbalances and their ideal values are primarily caused by deviations in the coupling coefficients M_{23}^{I} and M_{23}^{II}. In other words, the magnitude and phase imbalances are highly sensitive to the physical parameters d_{23} and d_{24}. And it can be improved by extracting coupling coefficients more accurately. Overall, the simulated predictions closely match the measured results, demonstrating the feasibility of the proposed design approach. Table 7 provides a comparison between the recently published microstrip balun diplexers and the proposed design. The table reveals that the proposed duplexing balun filter has the smallest circuit area (reduced by at least 22%), as compared to the designs in [13], [14], [23], [24], and [27], and still delivers commendable performance. Although the filtering balun-diplexer in [28] has a smaller size, the design freedom in terms of bandwidth and filter order is limited.

IV. CONCLUSION

In this paper, a design method for compact and multifunctional microwave balun filters and duplexing balun filters is proposed. Relevant theoretical analysis and detailed design steps have also been provided. This design integrates the functionality of multiple circuits into a single component, which can be advantageous for reducing circuit area and production costs. To validate its feasibility, this study actually designed and fabricated two balun filters and one duplexing balun filter, and the results from both simulation and measurement closely matched. Overall, the proposed microwave balun filters and duplexing balun filters offer advantages such as small size, low loss, high isolation, wide stopband, and low design complexity, making them well-suited for modern multiband and multiservice wireless communication systems.

REFERENCES

[1] J.-Y. Shao, S.-C. Huang, and Y.-H. Pang, "Wilkinson power divider incorporating quasi-elliptic filters for improved out-of-band rejection," *Electron. Lett.*, vol. 47, no. 23, p. 1288, 2011.

[2] P. Cheong, K.-I. Lai, and K.-W. Tam, "Compact Wilkinson power divider with simultaneous bandpass response and harmonic suppression," in *IEEE MTT-S Int. Microw. Symp. Dig.*, May 2010, pp. 1588–1591.

[3] Y. C. Li, Q. Xue, and X. Y. Zhang, "Single- and dual-band power dividers integrated with bandpass filters," *IEEE Trans. Microw. Theory Techn.*, vol. 61, no. 1, pp. 69–76, Jan. 2013.

[4] C.-F. Chen, T.-Y. Huang, T.-M. Shen, and R.-B. Wu, "Design of miniaturized filtering power dividers for system-in-a-package," *IEEE Trans. Compon., Packag., Manuf. Technol.*, vol. 3, no. 10, pp. 1663–1672, Oct. 2013.

[5] C.-F. Chen and C.-Y. Lin, "Compact microstrip filtering power dividers with good in-band isolation performance," *IEEE Microw. Wireless Compon. Lett.*, vol. 24, no. 1, pp. 17–19, Jan. 2014.

[6] C.-F. Chen, C.-Y. Lin, B.-H. Tseng, and S.-F. Chang, "Compact microstrip electronically tunable power divider with Chebyshev bandpass response," in *Proc. Asia–Pacific Microw. Conf.*, Nov. 2014, pp. 1291–1293.

[7] P.-L. Chi and T. Yang, "A 1.3–2.08 GHz filtering power divider with bandwidth control and high in-band isolation," *IEEE Microw. Wireless Compon. Lett.*, vol. 26, no. 6, pp. 407–409, Jun. 2016.

[8] X.-L. Zhao, L. Gao, X. Y. Zhang, and J.-X. Xu, "Novel filtering power divider with wide stopband using discriminating coupling," *IEEE Microw. Wireless Compon. Lett.*, vol. 26, no. 8, pp. 580–582, Aug. 2016.

[9] C.-H. Wu, C.-H. Wang, S.-Y. Chen, and C. Hsiung Chen, "Balanced-to-unbalanced bandpass filters and the antenna application," *IEEE Trans. Microw. Theory Techn.*, vol. 56, no. 11, pp. 2474–2482, Nov. 2008.

[10] T. Yang, M. Tamura, and T. Itoh, "Compact hybrid resonator with series and shunt resonances used in miniaturized filters and balun filters," *IEEE Trans. Microw. Theory Techn.*, vol. 58, no. 2, pp. 390–402, Feb. 2010.

[11] L. Kun Yeung and K.-L. Wu, "A dual-band coupled-line balun filter," *IEEE Trans. Microw. Theory Techn.*, vol. 55, no. 11, pp. 2406–2411, Nov. 2007.

[12] G.-S. Huang and C. H. Chen, "Dual-band balun bandpass filter with hybrid structure," *IEEE Microw. Wireless Compon. Lett.*, vol. 21, no. 7, pp. 356–358, Jul. 2011.

[13] C.-H. Wu, C.-H. Wang, and C. H. Chen, "A novel balanced-to-unbalanced diplexer based on four-port balanced-to-balanced bandpass filter," in *Proc. 38th Eur. Microw. Conf.*, Oct. 2008, pp. 28–31.

[14] Q. Xue, J. Shi, and J.-X. Chen, "Unbalanced-to-balanced and balanced-to-unbalanced diplexer with high selectivity and common-mode suppression," *IEEE Trans. Microw. Theory Techn.*, vol. 59, no. 11, pp. 2848–2855, Nov. 2011.

[15] C. Cai, J. Wang, L. Zhu, and W. Wu, "A new approach to design microstrip wideband balun bandpass filter," *IEEE Microw. Wireless Compon. Lett.*, vol. 26, no. 2, pp. 116–118, Feb. 2016.

[16] F. Huang, J. Wang, and L. Zhu, "A new approach to design a microstrip dual-mode balun bandpass filter," *IEEE Microw. Wireless Compon. Lett.*, vol. 26, no. 4, pp. 252–254, Apr. 2016.

[17] J. Wang, F. Huang, L. Zhu, C. Cai, and W. Wu, "Study of a new planar-type balun topology for application in the design of balun bandpass filters," *IEEE Trans. Microw. Theory Techn.*, vol. 64, no. 9, pp. 2824–2832, Sep. 2016.

[18] H. Tang, J.-X. Chen, H. Chu, G.-Q. Zhang, Y.-J. Yang, and Z.-H. Bao, "Integration design of filtering antenna with load-insensitive multilayer balun filter," *IEEE Trans. Compon., Packag., Manuf. Technol.*, vol. 6, no. 9, pp. 1408–1416, Sep. 2016.

[19] J.-X. Xu, X. Y. Zhang, and X.-L. Zhao, "Compact LTCC balun with bandpass response based on Marchand balun," *IEEE Microw. Wireless Compon. Lett.*, vol. 26, no. 7, pp. 493–495, Jul. 2016.

[20] L.-P. Feng and L. Zhu, "Compact wideband filtering balun using stacked composite resonators," *IEEE Access*, vol. 6, pp. 34651–34658, 2018.

[21] J. Zhou, H. J. Qian, J. Ren, and X. Luo, "Reconfigurable wideband filtering balun with tunable dual-notched bands using CPW-to-slot transition and varactor-loaded shorted-slot," *IEEE Access*, vol. 7, pp. 36761–36771, 2019.

[22] M. Du, K. Chen, J. Zhao, and Y. Feng, "Differential signal propagation in spoof plasmonic structure and its application in microwave filtering balun," *IEEE Access*, vol. 8, pp. 109009–109014, 2020.

[23] C.-M. Chen, S.-J. Chang, C.-F. Yang, and C.-Y. Chen, "A simple and effective method for designing frequency adjustable balun diplexer with high common-mode suppression," *IEEE Microw. Wireless Compon. Lett.*, vol. 25, no. 7, pp. 433–435, Jul. 2015.

[24] Z.-L. Wu, C.-H. Lee, and H.-H. Chen, "Balun diplexer design in hybrid structure of microstrip line and slot-line," in *Proc. Asia–Pacific Microw. Conf. (APMC)*, vol. 3, Dec. 2015, pp. 1–3.

[25] S.-W. Wong, J.-Y. Lin, H. Zhu, R.-S. Chen, L. Zhu, and Y. He, "Cavity balanced and unbalanced diplexer based on triple-mode resonator," *IEEE Trans. Ind. Electron.*, vol. 67, no. 6, pp. 4969–4979, Jun. 2020.

[26] L. Xu, W. Yu, and J.-X. Chen, "Unbalanced-/balanced-to-unbalanced diplexer based on dual-mode dielectric resonator," *IEEE Access*, vol. 9, pp. 53326–53332, 2021.

[27] H.-Y. Chen, C.-F. Chen, B.-Y. Su, C.-T. Chiang, Y.-F. Tsai, H.-Y. Yu, and W.-J. Li, "Integration design of filtering balun diplexer with improved output isolation performance," in *Proc. Asia–Pacific Microw. Conf. (APMC)*, Nov. 2022, pp. 527–529.

[28] H. Tian, H. Liu, S. Zheng, and T. Zuo, "Compact filtering balun-diplexer using coupled-line-loaded hairpin ring resonator," *IEEE Trans. Circuits Syst. II, Exp. Briefs*, vol. 70, no. 3, pp. 989–993, Mar. 2023.

[29] J. S. Hong and M. J. Lancaster, *Microstrip Filter for RF/Microwave Application*. New York, NY, USA: Wiley, 2001.

CHI-FENG CHEN (Member, IEEE) received the M.S. degree in electrophysics from National Chiao Tung University, Hsinchu, Taiwan, in 2003, and the Ph.D. degree in communication engineering from National Taiwan University, Taipei, Taiwan, in 2006.

From 2008 to 2010, he was an RF Engineer with Compal Communications Inc., Taipei, where he was involved in the research and development of global system for mobile communication (GSM) and code division multiple access (CDMA) mobile phones. In April 2010, he joined the Graduate Institute of Communication Engineering, National Taiwan University, as a Postdoctoral Research Fellow. Since 2012, he has been a Faculty Member with the Department of Electrical Engineering, Tunghai University (THU), Taichung, Taiwan, where he is currently a Professor. He is also the Chairperson of the Department of Electrical Engineering, THU. His research interests include the design of microwave circuits and associated RF modules for microwave and millimeter-wave applications.

YI-FANG TSAI was born in Yunlin, Taiwan, in 1978. She is currently pursuing the M.S. degree with the Department of Electrical Engineering, Tunghai University, Taichung, Taiwan. Her current research interest includes the design of RF/microwave circuits.

BAI-HONG CHEN was born in Taoyuan, Taiwan, in 1999. He is currently pursuing the M.S. degree with the Department of Electrical Engineering, Tunghai University, Taichung, Taiwan. His current research interest includes the design of RF/microwave circuits.

RUO-YIN YANG was born in Pingtung, Taiwan, in 1999. She is currently pursuing the M.S. degree with the Department of Electrical Engineering, Tunghai University, Taichung, Taiwan. Her current research interest includes the design of RF/microwave circuits.

YU-SHENG ZENG was born in Changhua, Taiwan, in 1998. He is currently pursuing the M.S. degree with the Department of Electrical Engineering, Tunghai University, Taichung, Taiwan. His current research interest includes the design of RF/microwave circuits.